Exploitation of Sb P-doped C3N4 and peroxidase immobilized on epoxidized linseed oil films for pollutant removal

Catalysis Science & Technology

ROYAL SOCIETY OF CHEMISTRY

PAPER

View Article Online
View Journal | View Issue

Cite this: *Catal. Sci. Technol.*, 2024, 14, 5086

Exploitation of Sb P-doped C_3N_4 and peroxidase immobilized on epoxidized linseed oil films for pollutant removal†

E. Gaggero,[a] M. Paturel,[b] F. Cristaudo, [a] R. Sesia,[c] M. Sangermano, [c] P. Calza *[a] and T. Ohno [d]

We utilized the combination of heterogeneous photocatalysis with soybean peroxidase (SBP) to allow the degradation of refractory pollutants. A self-standing system was developed *via* UV-curing by dispersing Sb P-doped C_3N_4 and SBP onto a bio-based film composed of epoxidized linseed oil. Peroxidase enzymes are activated by hydrogen peroxide that, in our system, is provided *via* coupling with a photocatalyst; specifically, the remarkable capability of atomically dispersed antimony P-doped carbon nitride in the hydrogen peroxide production was leveraged to create this hybrid material, establishing a self-sustaining system with limited use of reactants. 2,4-Dichlorophenol (DCP) was used as a target molecule to assess the degradative performances of the so-produced films, considering two scenarios: (a) films containing Sb P-doped C_3N_4 only and (b) films holding a layer of the photocatalyst and a layer of SBP. The multilayer film is the most efficient, with a fourfold increase in the kinetic constants compared to the film with the catalyst only. Experiments were also extended to a mixture of imidacloprid, DCP, diclofenac and bisphenol A in actual water, where the overall degradation efficiency remains high, and the multilayer film is reaffirmed as the most effective.

Received 11th April 2024,
Accepted 13th July 2024

DOI: 10.1039/d4cy00474d

rsc.li/catalysis

1. Introduction

In recent decades, population growth, urbanization and expansion of agricultural areas have led to a critical shortage of clean water resources, turning the resolution of the water crisis into a matter of paramount importance.[1] Water has become extensively contaminated through various routes, introducing new and potentially toxic pollutants, such as the so-called contaminants of emerging concern (CECs). CECs represent a broad class of pollutants, including but not limited to pharmaceuticals, personal care products, pesticides, industrial chemicals, endocrine-disrupting compounds, and other emerging contaminants,[2–4] that have gained attention in water quality management due to their potential impact on ecosystems and human health. Additionally, some CECs have the potential to bioaccumulate in living organisms, posing a threat as they move up the food chain. Traditional wastewater treatment plants are not always effective in removing CECs from water, since many of these compounds resist degradation during conventional treatment processes, leading to their release into receiving waters.[5–7] In the framework of water treatment, advanced oxidation processes (AOPs) had strong development especially in the removal of CECs. AOPs are applied in the treatment of various pollutants, including industrial wastewater containing persistent organic compounds, and are particularly effective in the degradation of recalcitrant and hard-to-treat pollutants. Hydroxyl radicals ($^{\bullet}OH$) are the primary reactive species in AOPs, but other reactive oxygen species such as superoxide radicals ($O_2^{\bullet-}$), singlet oxygen ($^1O_2$), and hydrogen peroxide (H_2O_2) may also contribute to the oxidation processes.[8] Hydrogen peroxide is harmless and widely used for the activation of hydroxyl radicals (·OH) in Fenton or Fenton-like processes.[9–11]

Considering heterogeneous photocatalysis, in most cases it results in the complete mineralization of organic carbon-containing compounds into water and CO_2.[12–15] Beyond the photocatalytic processes discussed so far, there are other innovative water treatment methods that take advantage of biological processes or membrane filtration, adsorption, or a combination of multiple strategies that allow the advantages of each technique to be combined and exploited synergistically. The efficiency of soya-extracted peroxidase extends to the

[a] *Department of Chemistry, University of Turin, Via Pietro Giuria 5, 10126 Turin, Italy. E-mail: paola.calza@unito.it*
[b] *Ecole Polytech Montpellier, France*
[c] *Department of Applied Science and Technology, Polytechnic of Turin, Corso Duca degli Abruzzi 24, 10129 Turin, Italy*
[d] *Department of Applied Chemistry, Faculty of Engineering, Kyushu Institute of Technology, 1-1 Sensuicho, Tobata, Kitakyushu, Japan*

† Electronic supplementary information (ESI) available. See DOI: https://doi.org/10.1039/d4cy00474d

degradation of phenolic substrates and exhibits remarkable resistance to high temperatures, maintaining activity at around 70 °C. This resilience makes soya-derived peroxidase not only attractive for industrial applications but also suitable for pollutant abatement.[16–18] Peroxidase enzymes are activated by hydrogen peroxide, which should be added to the system to ensure the oxidation of contaminants. However, the coupling with a photocatalyst, which produces hydrogen peroxide under irradiation, allows for obtaining a self-sustaining system that does not require additional reagents. In our previous papers,[19,20] we showed that the TiO_2 and ZnO based materials act synergistically with the enzyme soybean peroxidase (SBP) when dispersed within films or fibers, leading to an increase in the removal of selected pollutants, implying that the photocatalysts produced, under irradiation, enough H_2O_2 to activate SBP.

In the present work, we aim to go one step beyond by developing a photocatalyst capable to produce an enhanced amount of hydrogen peroxide. Attention has recently been focused on the potential for efficiently producing H_2O_2 through photocatalytic reaction processes, especially exploiting carbon nitride-based materials.[21,22] Nevertheless, the low efficiency of pristine g-C_3N_4 still limits its activity because of its high rate of charge recombination caused by defects introduced into the structure after polymerization, and low absorption of visible light, which leads to insufficient visible-light harvesting.[23–25]

To address these limitations, several protocols have been devised, encompassing morphological tuning, defect engineering, co-catalyst loading, semiconductor copolymerization, element doping, and hybridization. Each of these strategies aims to mitigate one or two drawbacks by altering specific properties of the pristine photoactive coordination network. These modifications include inhibiting charge recombination, narrowing the bandgap and/or enhancing light absorption, and introducing active sites conducive to the selective 2-electron oxygen reduction reaction ($2e^-$ ORR).[26]

The properties of g-C_3N_4 materials can be effectively altered through doping strategies involving the introduction of additional elements and impurities into the framework.[27] Furthermore, P-doping can induce a significant increase in visible light harvesting, narrowing of the band gap energy and a shift of the upper edge of the VB to a less positive value.[28] Recently, Ohno *et al.* developed a Sb single atom photocatalyst (Sb-SAPC) that achieved non-sacrificial photocatalytic H_2O_2 synthesis under visible light irradiation. The introduction of single Sb sites led to the accumulation of electrons, which acted as photoreduction sites for O_2 *via* a $2e^-$ ORR pathway.[29,30] The catalyst achieved non-sacrificial H_2O_2 production using water as an electron donor.

As a further step in the frame of sustainability, we prepared supported materials with the photocatalyst dispersed within bio-based UV-cured films. We have extensive experience in the preparation of UV-cured films from bio-based precursors.[31–34] This is of interest given the growing focus within the scientific community on reducing the use of fossil-based materials and promoting sustainability.[35] The exploitation of bio-based precursors from agricultural waste could be even more interesting from a circular economy point of view. Agro-food waste can be exploited to recover bio-based precursors, which can be easily functionalized and photocured in the form of films.

When the photocatalyst and the enzyme are dispersed within the polymeric network, the achieved materials could be used for water remediation. The use of the UV-curing method to prepare the supported catalyst material is particularly attractive since this polymerization process is environmentally friendly. The film was prepared starting from epoxidized linseed oil in the presence of a suitable cationic photoinitiator. The curing process is fast, occurs at room temperature and in the absence of any solvents; by UV irradiation it is possible to induce the polymer formation with a fast transformation of the liquid monomer into a solid film with tailored physical–chemical and mechanical properties.[36]

In this work, we prepare epoxidized linseed oil UV-cured films containing atomically dispersed antimony P-doped carbon nitride as the photocatalyst together with peroxidase enzyme and we explore the ability of the photocatalyst/enzyme systems to abate various pollutants. A bi-layer film was produced where the photocatalyst was dispersed in the first layer and the enzyme in the second one, to avoid their direct contact. During irradiation, the photocatalyst should produce enough H_2O_2 to activate the peroxidase enzyme. Therefore, as a preliminary step, we evaluated if the different supported photocatalysts dispersed within the polymeric network could produce enough H_2O_2 to activate the enzyme, and assessed if the enzyme did not lose its activity when dispersed in the polymer film or subjected to irradiation. The efficiency of the monolayer system was finally compared with the multilayer in actual water.

2. Materials and methods

2.1. Materials

The epoxidized linseed oil (Merginat ELO) was provided by HOBUM Oleochemicals GmbH. The typical parameters of this oleochemical epoxy compound based on linseed oil are oxirane content equal to 8.5–9.5%, maximum acid value equal to 1 mg KOH per g, viscosity between 700 and 1300 mPa × s at 25 °C, maximum iodine value equal to 7 g I_2/100 g and biobased carbon content equal to 100%. The cationic photoinitiator (triarylsulfonium hexafluoroantimonate salt), mixed 50 wt% in propylene carbonate, was purchased from Sigma-Aldrich. Ammonium dihydrogen phosphate, carbamazepine (>99%), melamine (99%), sodium hexafluoroantimonate(v), thiourea (99%), 4-aminoantipyrin, phenol (P), imidacloprid, carbamazepine, hydroquinone (HQ), 1,4-benzoquinone (BQ), 2,4-diclorophenol, diclofenac, bisphenol A, phosphoric acid (≥85.0%), acetonitrile and ethanol were purchased by Sigma-Aldrich. Peroxidase was purchased from Bio-Research Products Inc., Iowa-USA, and used without further purification.

All solutions were prepared with ultrapure water from a Millipore Milli-Q™ system (TOC < 2 ppb, conductivity ≥18 MΩ cm).

2.2. Synthesis and characterization of the photocatalysts

Sb(0.5) P-doped C_3N_4 and Sb(1) P-doped C_3N_4 materials, where Sb(0.5) and Sb(1) indicate Sb mmol, were prepared by wet chemical method synthesis as reported by Teng *et al.*[29] and briefly described in the ESI.† The materials have been fully characterized and the details are reported in the ESI.† XRD spectra are shown in Fig. S1,† while FESEM images and EDX details are shown in Fig. S2 and S3.†

2.3. Epoxidized linseed oil (ELO) film preparation and UV-curing characterization

ELO UV-cured films were achieved by adding 2 phr (parts per hundred resin) of the sulfonium salt as the cationic photoinitiator and irradiating with UV light (Dymax ECE 5000 lamp, light intensity 130 mW cm^{-2}). The embedded photocatalysts in the epoxy formulations were Sb(0.5) P-doped C_3N_4 (labelled Sb(0.5)) and Sb(1) P-doped C_3N_4 (labelled Sb(1)).

Fourier Transform Infrared (FTIR) spectroscopy analyses were performed to investigate the photoreactivity of ELO-based formulations, using a Thermo Scientific Nicolet iS50 FTIR spectrometer. The spectra were recorded in the range of 4000–600 cm^{-1} as 32 scans with a spectral resolution of 4.0 cm^{-1}. The FTIR instrument equipped with a diamond crystal ATR accessory was used to evaluate the composition of the formulation.

The conversion degree was assessed by the disappearance of the epoxy peaks centred at 846 and 823 cm^{-1}. The peak at 1744 cm^{-1}, assigned to the C═O stretching of ELO, was assumed to be unaffected by UV radiation and thus it was taken as the ref. 33. The conversion degree was calculated according to eqn (1).[37–40]

$$\text{Conversion } [\%] = \frac{\left(\frac{A_{\text{epoxy}}}{A_{\text{ref}}}\right)_{t=0} - \left(\frac{A_{\text{epoxy}}}{A_{\text{ref}}}\right)_{t}}{\left(\frac{A_{\text{epoxy}}}{A_{\text{ref}}}\right)_{t=0}} \times 100 \quad (1)$$

where A_{epoxy} and A_{ref} are the areas of the epoxy ring peak and the reference peak, respectively, evaluated at different times.

2.4. H_2O_2 production

The prepared films were tested for hydrogen peroxide production, using Milli-Q water as reaction medium, and irradiated with a 1500 W xenon lamp (Solarbox, CO.FO.ME. GRA., Milan, Italy) with a cut-off filter at 340 nm.

The concentration of produced hydrogen peroxide was monitored over time and determined by employing the horseradish peroxidase-coupled oxidation method described by Frew *et al.*[41] Hydrogen peroxide oxidatively couples with 4-aminoantipyrine and phenol, in the presence of peroxidase to yield a chromogen (a quinoneimine dye) with a maximum absorption at 505 nm.

2.5. Photocatalytic tests

To assess the degradative performances of UV-cured films containing either the photocatalyst or the photocatalyst and enzyme (multilayer film), the degradation tests were performed on solutions of 2,4-dichlorophenol (DCP) at 10 mg L^{-1} and carbamazepine at natural pH (pH = 7.1). Experiments were carried out in Pyrex glass cells kept under magnetic stirring and filled with 10 mL of the contaminant's solution and a rectangular film. The cells were irradiated in the sun simulator described in 2.4.

The photodegradation process was followed over time by sampling 100 μl of the solution after regular time intervals. For the degradation test performed with the multilayer films, the film was inserted inside the cell so that the side containing the photocatalyst faced upward and was effectively irradiated, while the side with the enzyme faced downward.

Analyses were performed with a Merck-Hitachi HPLC system equipped with an L-6200A Intelligent Pump, an L-4200 UV-vis detector and a six-way Rheodyne valve injection system. For carbamazepine analyses, the detection wavelength was set at 285 nm, eluting with 65% of phosphoric acid solution at pH 2.8 and 35% of acetonitrile at a flow rate of 1 mL min^{-1} (the retention time was 5.1 minutes). For 2,4-dichorophenol (DCP), the detection wavelength was set at 320 nm and the elution was performed with the same eluents in the ratio 1 : 1 at a flow rate of 1 mL min^{-1} (the retention time for DCP was 3.9 minutes, while for HQ, BQ and P were 1.53, 1.91 and 2.17 min, respectively).

After preliminary tests, degradation experiments were performed on a mixture of four pollutants (imidacloprid, 2,4-diclorophenol, diclofenac and bisphenol A) at natural pH (pH = 7.1). The concentration of each compound was 4 mg L^{-1}. The detection wavelength was set at 220 nm and a gradient elution was performed with a mixture of phosphoric acid solution at pH 2.8 (A) and acetonitrile (B) at a flow rate of 1 mL min^{-1} in accordance with the following program: 75 : 25 A/B for 3 min; 75 : 25 to 65 : 35 over 4 min; 65 : 35 to 40 : 60 over 8 min; 40 : 60 for 5 min; 40 : 60 to 75 : 25 over 0.5 min; 75 : 25 for 5 min.

The retention times were 4.30, 14.07, 14.80 and 18.20 min for imidacloprid, bisphenol A, 2,4-dichlorophenol and diclofenac, respectively. Experiments on the mixture were firstly conducted in Milli-Q water and then in fish farm water. Water from aquaculture was provided by UltraAQUA (Aalborg, Denmark); the parameters for the fish farm water are shown in Table S2 in the ESI.†

The acute toxicity of DCP and its transformation products was evaluated for three organisms (fish, daphnid, green algae) using the ECOSAR software v2.2. Chronic toxicity concentrations for these organisms were also computed using the same software.

3. Results

3.1. ELO film preparation and characterization

Fig. S4a† schematically shows the mechanism of ELO photocrosslinking. The embedded photocatalysts in the epoxy

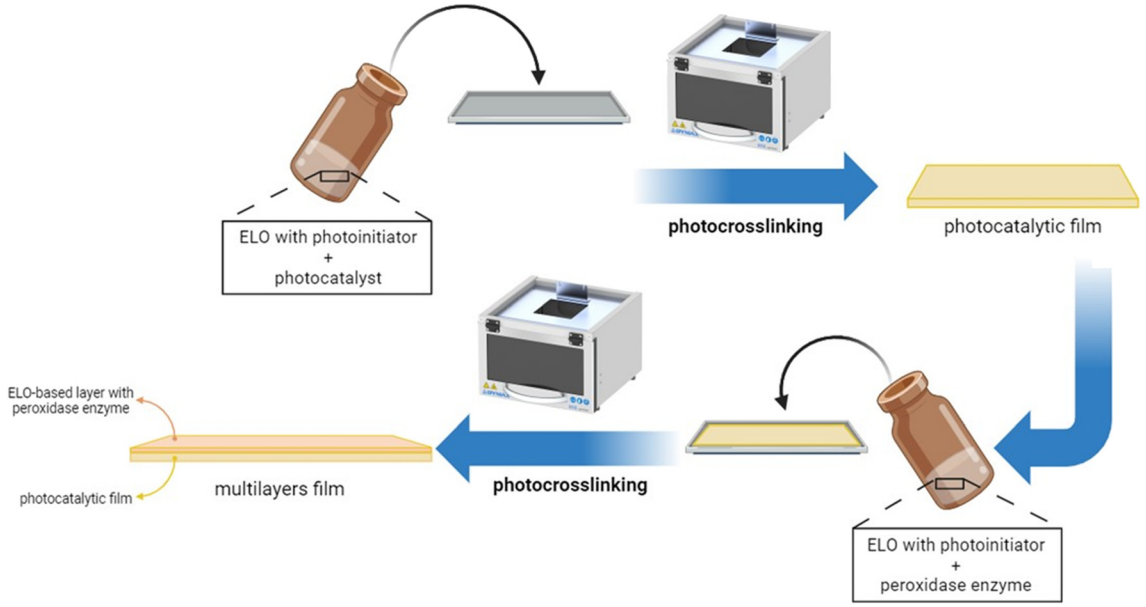

Fig. 1 ELO film preparation procedure.

formulations were Sb(0.5) P-doped C_3N_4 (named Sb(0.5)) and Sb(1) P-doped C_3N_4 (named Sb(1)). Films with different percentages of the photocatalyst, namely 0, 0.5, 1, 1.5, and 2 wt%, were prepared and preliminarily tested. Afterward, multilayer films were prepared by stratifying a layer containing the optimized quantity of the photocatalyst and a layer containing 0.5 phr of enzyme (see Fig. 1). Prepared ELO films, shown in Fig. S4b,† were rectangular in shape, about 1.5 × 0.8 cm, with a thickness of 0.5 and 1 mm for photocatalytic and multilayer films, respectively.

The cationic UV-curing of ELO-based films was monitored through real-time FTIR analysis. The real-time spectra of ELO formulation before and after UV light irradiation are shown in Fig. 2. The two peaks observed at 2926 cm^{-1} and 2854 cm^{-1} can be attributed to the stretching vibrations of methylene groups' asymmetrical and symmetrical –CH_2– bonds, respectively. The peak at 1745 cm^{-1} is attributed to the stretching vibration of the –C═O ester group. The peaks at 1465 cm^{-1} and 1378 cm^{-1} can be attributed to the scissoring and rocking vibrations of the –C–H (CH_2, CH_3) groups and –C–H (CH_2) group, respectively. The peaks at 1162 cm^{-1} and 1116 cm^{-1} are associated with the bending and stretching vibrations of the –C–O bonds. The double peak observed at 840 cm^{-1} is attributed to the C–O–C bonds in the epoxy ring.[38,39,42–44]

As shown in Fig. 2, the successful photopolymerization of ELO is confirmed by the disappearance of the peaks centred

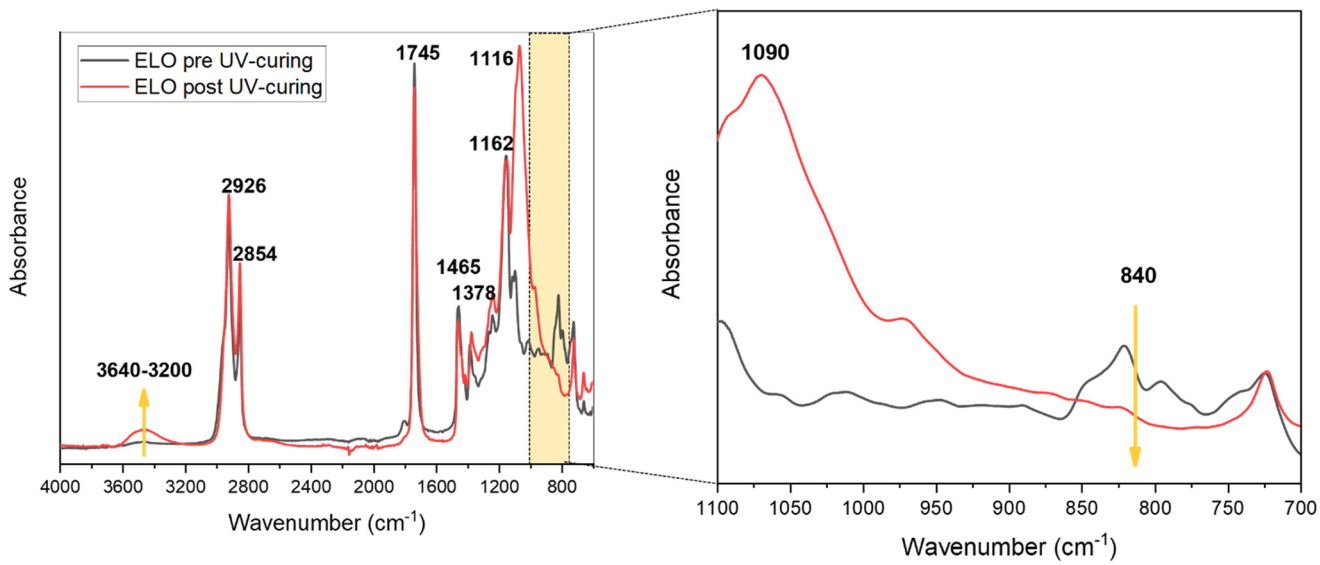

Fig. 2 Real-time FTIR of ELO pre- and post-photocuring.

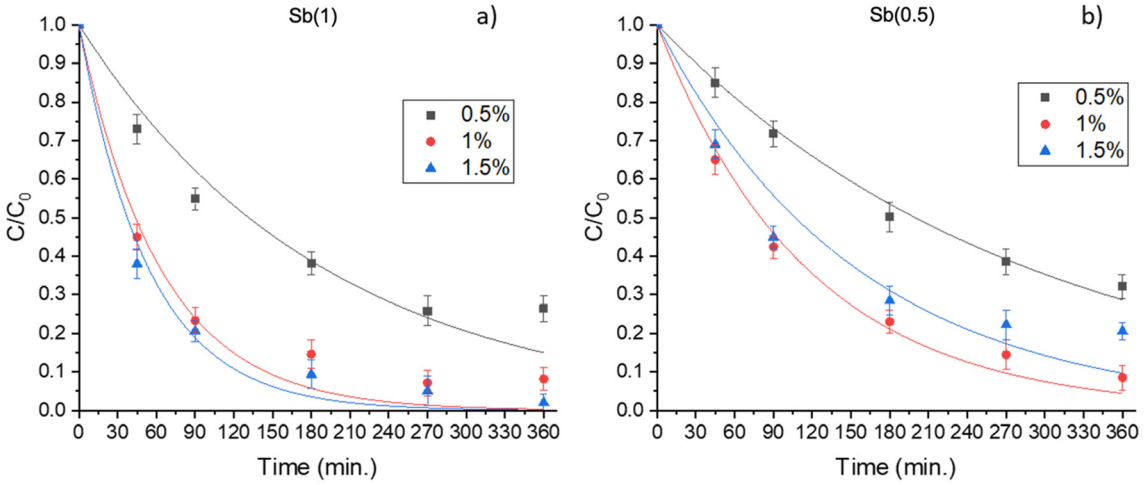

Fig. 3 2,4-Dichlorophenol degradation using films containing different photocatalysts: a) Sb(1) P-doped C_3N_4 (Sb(1)) and b) Sb(0.5) P-doped C_3N_4 (Sb(0.5)).

at 840 cm^{-1} after irradiation due to the epoxy ring opening reaction. Instead, due to the epoxy ring opening, and thus the formation of the polymeric network (Fig. S4†), two new peaks emerge—one centred at 1090 cm^{-1}, associated with the ether stretching vibration of C–O–C, and the other, a broad peak centred at 3465 cm^{-1}, indicative of the stretching vibration of the –OH hydroxyl group.[2,33,38–40,45–47]

Based on the area of the epoxy groups' peaks, the percentage of conversion degree as a function of irradiation time was calculated and plotted as shown in Fig. S5,† where the almost complete conversion is achieved after 180 seconds of irradiation and the conversion degree of the resin reached around 88%.

Similar results were achieved when the different photocatalysts and enzyme were dispersed in the photocurable formulation, which is clear evidence of the suitability of the UV-curing process to produce the supported photocatalyst/enzyme system.

3.2. Photocatalytic film: hydrogen peroxide production and pollutant abatement.

The photocatalytic efficiency of films containing different percentages of the photocatalysts (ranging from 0.5 to 1.5%) was tested using 2,4-dichlorophenol (DCP) at 10 mg L^{-1}, a pollutant frequently used as a target molecule in photocatalytic tests.[48–53]

Preliminarily, the pollutant adsorption in the dark was investigated on the pristine film and on the one with the highest percentage of photocatalyst (1.5%) by keeping DCP and the film in contact under magnetic stirring for sixteen hours; in both cases, adsorption was negligible.

To assess the photocatalytic performances of the so-produced films, degradation tests on DCP were performed under simulated solar light considering two scenarios: (a) monolayer films of the selected photocatalyst and (b) multilayer films containing a layer of photocatalyst and a layer of SBP.

Considering monolayer films, Fig. 3 shows the degradation curves obtained with films containing different percentages of Sb(0.5) or Sb(1). The results showed that, in both cases, the degradation efficiency is higher when 1 or 1.5% of the catalyst is dispersed in the film. The best performance is achieved in the case of Sb(1), where it can be inferred that the optimal percentage was 1.5 wt%, leading to the complete abatement of DCP in five hours of irradiation. Conversely, in the case of Sb(0.5), the removal is not complete in the considered time window (6 hours).

Similar results were also obtained when using carbamazepine as a target molecule (see Fig. S6†), where with Sb(1) an almost complete removal is obtained after 4 h of irradiation.

Hydrogen peroxide production was then monitored in the presence of Sb(05) and Sb(1) dispersed in aqueous solution or integrated in the epoxidized linseed oil film; the results are plotted as shown in Fig. 4.

In the case of the photocatalysts dispersed in an aqueous milieu, the production of H_2O_2 progresses steadily at the beginning of the reaction. While pristine g-C_3N_4 has little ability to produce H_2O_2, especially under visible light irradiation (see literature data collected in Table 1), and the addition of sacrificial agents such as alcohols is essential for the H_2O_2 generation, Sb(0.5) and Sb(1) generate H_2O_2 with a high

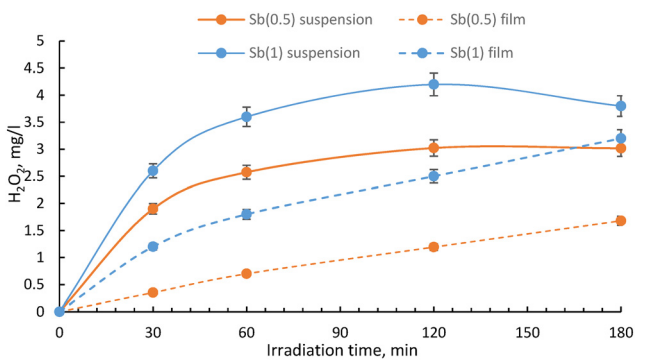

Fig. 4 H_2O_2 production from Sb(0.5) and Sb(1) dispersed in solution and in the film (1.5% of catalyst).

Table 1 Comparison of H_2O_2 production with other photosynthetic routes in the recent literature

Photocatalyst	Form	H_2O_2 production (μM) in 1 h	Light source	Ref.
TiO_2 (P25)	Film 3% wt	7	365 nm	19
TiO_2 (P25)	Suspension	1		
Ce–ZnO	Suspension	30	360 nm	20
ZnO	Suspension	20		
TiO_2 (P25)	Suspension	13		
Pristine C_3N_4	Suspension	29	Vis ($420 < \lambda < 800$ nm)	30
P-doped C_3N_4	Suspension	88		
Sb(1) P-dopedC_3N_4	Suspension	294		
Pristine C_3N_4	Suspension	147	UV-vis ($340 < \lambda < 800$ nm)	
P-doped C_3N_4	Suspension	118		
Sb(1) P-dopedC_3N_4	Suspension	706		
Sb(1) P-doped C_3N_4	Suspension	1058	UV-vis ($340 < \lambda < 800$ nm)	Present work
Sb(1) P-doped C_3N_4	Film 1.5%	529		
P-doped C_3N_4	Hollow spheres	35–90	Vis ($420 < \lambda < 800$ nm), O_2 saturated	54
PEI-GCN/Au (biomimetic photocatalysis)	Suspension	270	Vis ($420 < \lambda < 800$ nm)	55
P-doped C_3N_4	Suspension	52	Vis ($420 < \lambda < 800$ nm)	56

efficiency using water as an electron source and do not require the addition of sacrificial agents. As the concentration of H_2O_2 increases, two reverse reactions progressed in which H_2O_2 reacts with the holes to produce O_2, or H_2O_2 is further reduced by excited electrons to produce H_2O. Finally, these reactions reach an equilibrium state, so that the H_2O_2 production reaction is almost stopped.

On the other hand, the photocatalytic films show a slower evolution rate coupled with an increase in the production of hydrogen peroxide extended to longer irradiation times, suggesting that the reverse reaction is suppressed by the diffusion of the generated hydrogen peroxide from the film into the solution. Immobilization of the photocatalyst in the film led to a reduction in the rate of hydrogen peroxide formation, probably because the encapsulation of the nanoparticles in the film diminishes the ability of the catalyst surface to come in contact with oxygen and protons. However, while photocatalysts in powder require processes such as filtration after the reaction, its encapsulation in the film allows easy separation of the photocatalytic composite film at the end of the process.

Regarding the coupling with peroxidase, although the incorporation into the films caused a decrease in H_2O_2 production compared to the catalyst dispersed in aqueous solution, significant hydrogen peroxide generation was also confirmed when incorporated into the epoxidized linseed oil film. In particular, the film with Sb(1) produced the greatest amount of H_2O_2 (3 mg L^{-1} after 3 hours of irradiation), followed by Sb(0.5) (2 mg L^{-1} after 3 hours). It has to be pointed out that the present production of H_2O_2 is higher than the results shown in previous papers,[19,20] *e.g.* with supported TiO_2 or ZnO (H_2O_2 production passed from 7 μM h^{-1} for a TiO_2 film to 529 μM h^{-1} for a Sb(1) film).

3.3. Multilayer film: pollutant abatement

Multilayer films were then prepared by combining a first layer with 0.5% peroxidase enzyme, placed on the bottom side and sheltered from irradiation, with the best photocatalytic monolayer, namely 1.5% Sb(1), put on the top side and exposed to simulated sunlight. This configuration allows to protect the enzyme from illumination, allowing to maintain its activity for a longer time, and to prevent a direct interaction with the photocatalyst with the potential to promote the degradation of the enzyme itself.

DCP degradation was evaluated in three conditions, namely with the Sb(1) film only, the film in combination with the peroxidase enzyme in an aqueous solution, and the multilayer structure that encapsulates the enzyme within it; the calculated pseudo-first-order kinetic constants are displayed in Fig. 5.

The film showing the best performance is the multilayer, implying that the amount of hydrogen peroxide produced by the catalyst is adequate for allowing the enzyme to accomplish its oxidative activity.

The enhanced degradation efficiency could be explained by the occurrence of a joint attach by the photocatalyst and the enzyme, schematically described in Scheme 1.

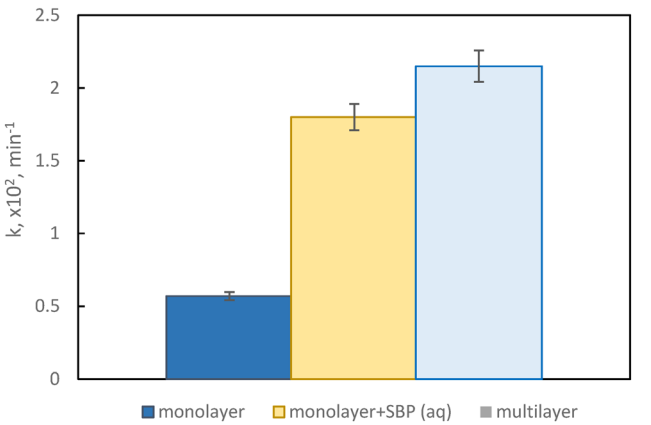

Fig. 5 Kinetic constants obtained from DCP using different photocatalytic films in three different conditions: the catalyst in a monolayer, coupled with peroxidase enzyme in solution and in multilayer films.

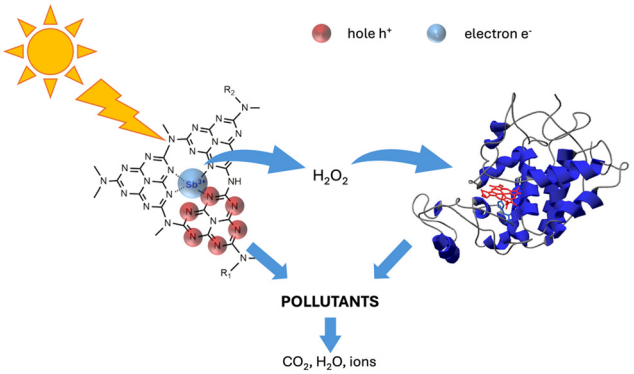

Scheme 1 The proposed mechanism of the photocatalytic and enzymatic processes.

The kinetic constant obtained with the multilayer film exhibits a fourfold increase compared to the film with catalyst only, thanks to the synergistic occurrence of these two processes; furthermore, the performance obtained with the multilayer configuration resembles the one obtained with the catalyst only plus the enzyme added to the aqueous solution, underscoring the remarkable success in crafting this film type.

The transformation of DCP proceeds through the formation of hydroquinone (HQ), 1,4-benzoquinone (BQ) and phenol (P) as by-products. While P is formed in trace amounts in all cases, BQ is the major intermediate when employing the multilayer film. This result is not surprising as it is well known that SBP catalyses phenol oxidation and allows the formation of benzoquinone derivatives.[57] *In silico* toxicity studies, collected as shown in Table S3,† pointed out that while BQ is more toxic than DCP toward fish and green algae, HQ and P are less toxic than DCP for all the tested microorganisms.

The possibility to reuse the multilayer film for further degradation trials has been explored as well. Reuse experiments were performed on the Sb(1) multilayer film for 3 cycles and the results of the photocatalytic tests performed on the DCP removal are shown in Fig. S7;† after 3 cycles of reuse, a reduction of around 30% in the photoactivity can be observed.

3.4. Abatement of a mixture of contaminants in actual water

The efficacy of the developed multilayer films was also evaluated in tackling a more intricate blend of emerging contaminants spanning diverse classes. A mixture of four contaminants (bisphenol A, diclofenac, imidacloprid and DCP) was investigated. Initially, the tests were conducted using Milli-Q water, followed by investigation with actual water sourced from an aquaculture facility. This expanded testing matrix aimed to provide a more comprehensive understanding of the films' performance in a real scenario with varying contaminant compositions.

We considered the multilayer films incorporating Sb(1) or Sb(0.5) in the ratio optimized earlier and the calculated kinetic constants are displayed in Fig. 6(left) and collected as shown in Table 2. Notably, the complete removal of bisphenol A (BPA) over the time considered is only accomplished with the most effective multilayer film, namely Sb(1) (see Fig. 7). Conversely, diclofenac (DIC) undergoes complete degradation in two hours, whereas imidacloprid (IMC) displays the least susceptibility to degradation.

Analysing the kinetic constants depicted in Fig. 6(right) for experiments accomplished in aquaculture water, a pattern akin to that observed in Milli-Q water is evident. The heightened complexity of the matrix brought a general reduction in the kinetic constants, particularly remarkable in the case of diclofenac, where the kinetic constant of degradation is halved with Sb(1). Nevertheless, the overall degradation efficiency remains satisfactory, and the film comprising Sb(1) P-doped C_3N_4 and peroxidase enzyme is reaffirmed as the most effective.

The reason for the decrease in the photocatalytic decomposition activity of Sb(1) films when using water from

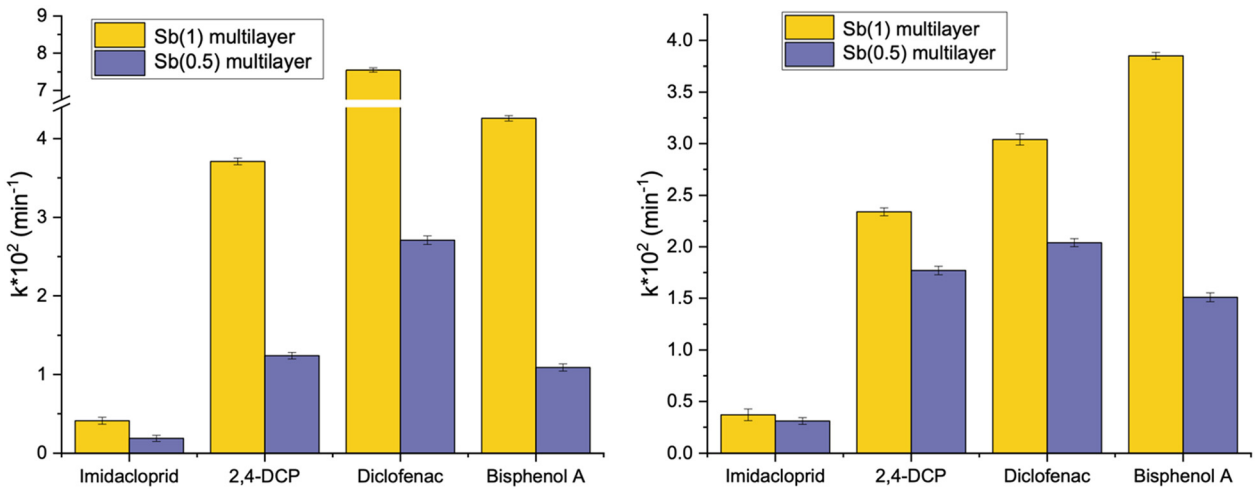

Fig. 6 Pseudo-first order kinetic constants derived by degradation curves of the pollutant's mixture in Milli-Q water (left) and aquaculture water (right).

Table 2 Pseudo-first order kinetic constants of degradation curves obtained using different multilayer films on the four pollutant mixture both in Milli-Q and aquaculture matrices

		$k \times 10^2$ (min^{-1})			
Matrix	Multilayer	IMC	DCP	DIC	BPA
Milli-Q	Sb(1)	0.41	3.71	7.55	4.26
Aquaculture	Sb(1)	0.37	2.34	3.05	3.89
Milli-Q	Sb(0.5)	0.19	1.24	2.71	1.10
Aquaculture	Sb(0.5)	0.31	1.77	2.04	1.51

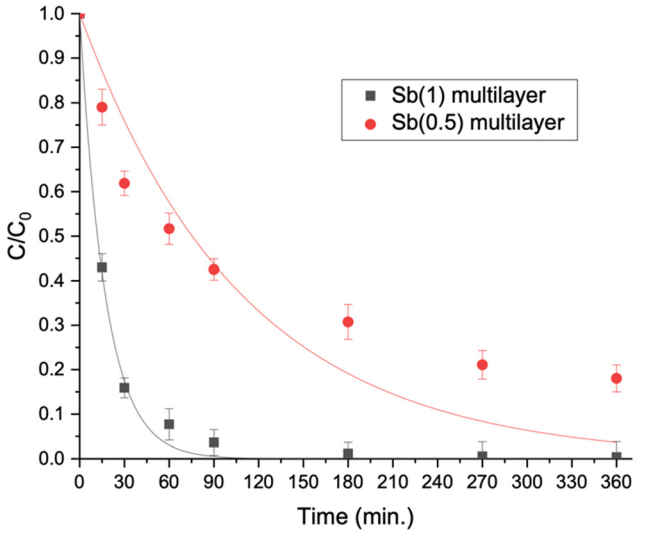

Fig. 7 Bisphenol A degradation curves obtained using different multilayer films on the pollutant's mixture solution.

aquaculture facilities is thought to be that various pollutants other than the decomposition target substances are dissolved in the water of aquaculture facilities. Therefore, the OH radicals generated when hydrogen peroxide supplied from the photocatalyst is decomposed by peroxidase are consumed by pollutants contained in water in addition to the decomposition target substance, so the decomposition activity of the decomposition target substance appears to be low. Analysis of these photocatalytic activities is an important index for evaluating and predicting the photocatalytic performance in real environments where various pollutants are present.

4. Conclusions

The remarkable capabilities of the developed photocatalyst and, more significantly, the hydrogen peroxide production observed in Sb P-doped C_3N_4 materials, were exploited to create a hybrid system. The optimal percentages of photocatalysts embedded in the epoxidized linseed oil film range from 1 to 1.5 wt% and exhibited a significant production of hydrogen peroxide, in turn employed by the peroxidase enzyme to accomplish pollutant degradation.

An autonomous enzyme system was therefore developed, working in synergy with the reactive oxygen species (ROS) produced in the presence of the photocatalyst, both supported on a multilayer bio-based film. The effectiveness of the developed multilayer films in degrading a variety of contaminants is also confirmed in an actual water sample from an aquaculture facility. In the real scenario, a general reduction in the kinetic constants was observed, but the overall degradation efficiency remained high, with Sb(1) P-doped C_3N_4 and peroxidase enzyme confirmed as the most effective combination.

This system offers several benefits in terms of both sustainability and convenience. Notably, the support material is entirely derived from bio-based sources, serving as a substitute for petroleum-based resins typically used in thermoset fabrication. The cationic UV-curing employed in the film fabrication process presents numerous advantages compared to traditional thermal curing methods. Specifically, photopolymerization results in minimal volatile emissions, rapid curing rates, and no shrinkage. Additionally, the absence of the need for additional heating makes this technique cost-effective. Furthermore, the system is self-standing, and uses the solar spectrum as its source of irradiation. Moreover, the films can be easily recovered and reused.

Data availability

The data supporting this article have been included as part of the ESI.†

Conflicts of interest

There are no conflicts to declare.

Acknowledgements

This research was funded by funding from the European Union's Horizon 2020 Research and Innovation Programme under the Marie Skłodowska-Curie Grant Agreement No. 101007578 (SusWater).

References

1 *IPCC: Climate change 2022: impacts, adaptation and vulnerability; IPCC: 2022*], ed. H.-O. Pörtner, D. C. Roberts, M. Tignor, E. S. Poloczanska, K. Mintenbeck, A. Alegría, M. Craig, S. Langsdorf, S. Löschke, V. Möller, A. Okem and B. Rama. Cambridge University Press, Cambridge, UK and New York, NY, USA, p. 3056.
2 J. Sanchez-Salas, D. Flores and E. R. Bandala, *Water Contamination: Sources, A.; Remediation*, Nova Science Publishers Inc., Hauppauge, N., USA, Water recalcitrant contaminants: Sources, assessment and remediation, 2018, pp. 1–76.
3 G. Lofrano, G. Libralato, S. Meric, V. Vaiano, O. Sacco, V. Venditto, M. Guida and M. Carotenuto, Occurrence and potential risks of emerging contaminants in water, in *Visible*

Light Active Structured Photocatalysts for the Removal of Emerging Contaminants, ed. O. Sacco and V. Vaiano, Elsevier, 2020, pp. 1–25.

4 A. Gogoi, P. Mazumder, V. K. Tyagi, G. T. Chaminda, A. K. An and M. Kumar, Occurrence and fate of emerging contaminants in water environment: a review, *Groundw. Sustain. Dev.*, 2018, **6**, 169–180.

5 D. Yadav, S. Rangabhashiyam, P. Verma, P. Singh, P. Devi, P. Kumar, C. M. Hussain, G. K. Gaurav and K. S. Kumar, Environmental and health impacts of contaminants of emerging concerns: Recent treatment challenges and approaches, *Chemosphere*, 2021, **272**, 129492.

6 L. Rizzo, S. Malato, D. Antakyali, V. G. Beretsou, M. B. Đolić, W. Gernjak, E. Heath, I. Ivancev-Tumbas, P. Karaolia, A. R. L. Ribeiro, G. Mascolo, C. S. McArdell, H. Schaar, A. M. T. Silva and D. Fatta-Kassinos, Consolidated vs new advanced treatment methods for the removal of contaminants of emerging concern from urban wastewater, *Sci. Total Environ.*, 2019, **655**, 986–1008.

7 O. Golovko, S. Örn, M. Sörengård, K. Frieberg, W. Nassazzi, F. Y. Lai and L. Ahrens, Occurrence and removal of chemicals of emerging concern in wastewater treatment plants and their impact on receiving water systems, *Sci. Total Environ.*, 2021, **754**, 142122.

8 P. Kumari and A. Kumar, ADVANCED OXIDATION PROCESS: A remediation technique for organic and non-biodegradable pollutant, *Results in Surfaces and Interfaces*, 2023, **11**, 100122.

9 Q. You, C. Zhang, M. Cao, B. Wang, J. Huang, Y. Wang, S. Deng and G. Yu, Defects controlling, elements doping, and crystallinity improving triple-strategy modified carbon nitride for efficient photocatalytic diclofenac degradation and H2O2 production, *Appl. Catal., B*, 2023, **321**, 1219421.

10 L. Zhou, W. Song, Z. Chen and G. Yin, Degradation of Organic Pollutants in Wastewater by Bicarbonate-Activated Hydrogen Peroxide with a Supported Cobalt Catalyst, *Environ. Sci. Technol.*, 2013, **47**(8), 3833–3839.

11 J. Xie, J. Jing, J. Gu, J. Guo, Y. Li and M. Zhou, Hydrogen peroxide generation from gas diffusion electrode for electrochemical degradation of organic pollutants in water: A review, *J. Environ. Chem. Eng.*, 2022, **10**(3), 107882.

12 S. H. S. Chan, T. Yeong Wu, J. C. Juan and C. Y. Teh, Recent developments of metal oxide semiconductors as photocatalysts in advanced oxidation processes (AOPs) for treatment of dye waste-water, *J. Chem. Technol. Biotechnol.*, 2011, **86**(9), 1130–1158.

13 H. Anwer, A. Mahmood, J. Lee, K.-H. Kim, J.-W. Park and A. C. K. Yip, Photocatalysts for degradation of dyes in industrial effluents: Opportunities and challenges, *Nano Res.*, 2019, **12**(5), 955–972.

14 S. Malato, P. Fernández-Ibáñez, M. I. Maldonado, J. Blanco and W. Gernjak, Decontamination and disinfection of water by solar photocatalysis: Recent overview and trends, *Catal. Today*, 2009, **147**(1), 1–59.

15 S. Patial, R. Kumar, P. Raizada, P. Singh, Q. Van Le, E. Lichtfouse, D. Le Tri Nguyen and V.-H. Nguyen, Boosting light-driven CO_2 reduction into solar fuels: Mainstream avenues for engineering ZnO-based photocatalysts, *Environ. Res.*, 2021, **197**, 111134.

16 J. K. A. Kamal and D. V. Behere, Thermal and conformational stability of seed coat soybean peroxidase, *Biochemistry*, 2002, **41**(29), 9034–9042.

17 J. S. Gray, B. Y. Yang, S. R. Hull, D. P. Venzke and R. Montgomery, The glycans of soybean peroxidase, *Glycobiology*, 1996, **6**(1), 23–32.

18 A. Henriksen, O. Mirza, C. Indiani, K. Teilum, G. Smulevich, K. G. Welinder and M. Gajhede, Structure of soybean seed coat peroxidase: A plant peroxidase with unusual stability and haem-apoprotein interactions, *Protein Sci.*, 2001, **10**(1), 108–115.

19 P. Calza, P. Avetta, G. Rubulotta, M. Sangermano and E. Laurenti, TiO2-Soybean Peroxidase composite materials as a new photocatalytic system, *Chem. Eng. J.*, 2014, **239**, 87–92.

20 M. Sarro, N. P. Gule, E. Laurenti, R. Gamberini, M. C. Paganini, P. E. Mallon and P. Calza, ZnO-based materials and enzymes hybrid systems as highly efficient catalysts for recalcitrant pollutants abatement, *Chem. Eng. J.*, 2018, **334**, 2530–2538.

21 S. Li, G. Dong, R. Hailili, L. Yang, Y. Li, F. Wang, Y. Zeng and C. Wang, Effective photocatalytic H_2O_2 production under visible light irradiation at g-C3N4 modulated by carbon vacancies, *Appl. Catal., B*, 2016, **190**, 26–35.

22 L. Zhou, J. Lei, F. Wang, L. Wang, M. R. Hoffmann, Y. Liu, S.-I. In and J. Zhang, Carbon nitride nanotubes with in situ grafted hydroxyl groups for highly efficient spontaneous H2O2 production, *Appl. Catal., B*, 2021, **288**, 119993.

23 W. J. Ong, L. L. Tan, Y. H. Ng, S. T. Yong and S. P. Chai, Graphitic Carbon Nitride ($g\text{-}C_3N_4$)-Based Photocatalysts for Artificial Photosynthesis and Environmental Remediation: Are We a Step Closer to Achieving Sustainability?, *Chem. Rev.*, 2016, **116**(12), 7159–7329.

24 F. K. Kessler, Y. Zheng, D. Schwarz, C. Merschjann, W. Schnick, X. Wang and M. J. Bojdys, Functional carbon nitride materials—design strategies for electrochemical devices, *Nat. Rev. Mater.*, 2017, 17030.

25 Y. Shiraishi, S. Kanazawa, Y. Sugano, D. Tsukamoto, H. Sakamoto, S. Ichikawa and T. Hirai, Highly selective production of hydrogen peroxide on graphitic carbon nitride (g-C3N4) photocatalyst activated by visible light, *ACS Catal.*, 2014, **4**(3), 774–780.

26 Z. Teng, W. Cai and T. Ohno, Functionalized Graphitic Carbon Nitrides for Photocatalytic H_2O_2 Production: Desired Properties Leading to Rational Catalyst Design, *Kona Powder Part. J.*, 2023, **40**, 124–148.

27 X. Liu, R. Ma, L. Zhuang, B. Hu, J. Chen, X. Liu and X. Wang, Recent developments of doped $g\text{-}C_3N_4$ photocatalysts for the degradation of organic pollutants, *Crit. Rev. Environ. Sci. Technol.*, 2020, **51**, 751–790.

28 M. Bellardita, E. I. García-López, G. Marcì, I. Krivtsov, J. R. García and L. Palmisano, Selective photocatalytic oxidation of aromatic alcohols in water by using P-doped $g\text{-}C_3N_4$, *Appl. Catal., B*, 2018, **220**, 222–233.

29 Z. Teng, Q. Zhang, H. Yang, K. Kato, W. Yang, Y.-R. Lu, S. Liu, C. Wang, A. Yamakata, C. Su, B. Liu and T. Ohno,

Atomically dispersed antimony on carbon nitride for the artificial photosynthesis of hydrogen peroxide, *Nat. Catal.*, 2021, **4**, 374–384.

30 E. Gaggero, W. Cai, P. Calza and T. Ohno, Enhanced hydrogen peroxide production and organic substrates degradation using atomically dispersed antimony P-doped carbon nitride photocatalysts, *Surf. Interfaces*, 2024, **48**, 104143.

31 L. Pezzana, E. Malmström, M. Johansson and M. Sangermano, UV-Curable Bio-Based Polymers Derived from Industrial Pulp and Paper Processes, *Polymers*, 2021, **13**(9), 1530–1556.

32 L. Pezzana, G. Melilli, G. Nathanaël, N. Sbirrazzuoli and M. Sangermano, Cationic UV Curing of Bioderived Epoxy Furan-Based Coatings: Tailoring the Final Properties by In Situ Formation of Hybrid Network and Addition of Monofunctional Monomer, *ACS Sustainable Chem. Eng.*, 2021, **9**, 17403–17412.

33 L. Pezzana, G. Melilli, P. Delliere, D. Moraru, N. Guigo, N. Sbirrazzuoli and M. Sangermano, Thiol-ene biobased networks: Furan allyl derivatives for green coating applications, *Prog. Org. Coat.*, 2022, **173**, 107203.

34 L. Pezzana, A. Emanuele, R. Sesana, C. Delprete, E. Malmström, M. Johansson and M. Sangermano, Cationic UV-curing of isosorbide-based epoxy coating reinforced with macadamia nutshell powder, *Prog. Org. Coat.*, 2023, **185**, 107949.

35 R. Geyer, J. R. Jambeck and K. L. Law, Production, use, and fate of all plastics ever made, *Sci. Adv.*, 2017, **3**(7), 1–5.

36 M. Sangermano, N. Razza and J. V. Crivello, Cationic UV-Curing: Technology and Applications, *Macromol. Mater. Eng.*, 2014, **299**, 775–793.

37 J. V. Crivello and R. Narayan, Epoxidized triglycerides as renewable monomers in photoinitiated cationic polymerization, *Chem. Mater.*, 1992, **4**, 692–699.

38 R. Sesia, A. G. Cardone, S. Ferraris, S. Spriano and M. Sangermano, Exploitation of tannic acid as additive for adhesion enhancement of UV-curable bio-based coating, *Prog. Org. Coat.*, 2024, **189**, 108311.

39 C. Noè, M. Hakkarainen and M. Sangermano, Cationic UV-curing of epoxidized biobased resins, *Polymers*, 2021, **13**, 89.

40 X. Ren, T. Xu, J. Thomas and M. D. Soucek, Isoprene soya diels–alder adduct and epoxidation for photopolymerization, *Macromol. Chem. Phys.*, 2021, **222**, 2100054.

41 J. E. Frew, P. Jones and G. Scholes, Spectrophotometric determination of hydrogen peroxide and organic hydropheroxides at low concentrations in aqueous solution, *Anal. Chim. Acta*, 1983, **155**, 139–150.

42 J. Chen, M. D. Soucek, W. J. Simonsick and R. W. Celikay, Synthesis and photopolymerization of norbornyl epoxidized linseed oil, *Polymer*, 2002, **43**, 5379–5389.

43 C. Mendes-Felipe, R. Cofano, A. Garcia, M. Sangermano and S. Lanceros-Mendeza, Photocurable 3D printed anisotropic electrically conductive materials based on bio-renewable composites, *Addit. Manuf.*, 2023, **78**, 103867.

44 C. Mendes-Felipe, P. Costa, I. Roppolo, M. Sangermano and S. L. Mendez, Bio-based Piezo- and Thermo-Resistive Photo-Curable Sensing Materials from Acrylated Epoxidized Soybean Oil, *Macromol. Mater. Eng.*, 2022, **307**, 2100934.

45 C. Noè, L. Iannucci, S. Malburet, A. Graillot, M. Sangermano and S. Grassini, New UV-Curable Anticorrosion Coatings from Vegetable Oils, *Macromol. Mater. Eng.*, 2021, **306**, 2100029.

46 L. Papadopoulos, L. Pezzana, N. Malitowski, M. Sangermano, D. Bokharis and T. Robert, UV-curing additive manufacturing of bio-based thermosets – effect of diluent concentration on printing and material properties of itaconic acid-based materials, *ACS Omega*, 2023, **8**, 31009–31020.

47 C. Decker, T. Nguyen Thi Viet and H. Pham Thi, Photoinitiated cationic polymerization of epoxides, *Polym. Int.*, 2001, **50**, 986–997.

48 P. Veerakumar, A. Sangili, S. M. Chen, R. Suresh Kumar, G. Arivalagan, M. Jannathul Firdhouse, K. Shahul Hameed and S. Sivakumar, Photocatalytic degradation of phenolic pollutants over palladium-tungsten trioxide nanocomposite, *Chem. Eng. J.*, 2024, **489**, 151127.

49 Q. Yang, X. Li, S. Zhang, W. Xu, X. Guo, X. Gao and Z. Jia, ZnO hierarchical structures with tunable oxygen vacancies for high performance in photocatalytic degradation of phenol, *J. Mol. Struct.*, 2024, **1304**, 137656.

50 Y. Zhang, Y. Li and S. Tabassum, Based on nanocomposites for degradation of phenolic compounds from aqueous environments by advanced oxidation processes: A review, *J. Water Process Eng.*, 2024, **61**, 105286.

51 Z. Cui, R. Yuan, H. Chen, B. Zhou, B. Zhu and C. Zhang, Application of polyaniline-based photocatalyst in photocatalytic degradation of micropollutants in water: A review, *J. Water Process Eng.*, 2024, **59**, 104900.

52 L. Tan, H. Feng, L. Li, H. Lin and J. Xiong, Phenol degradation by a combined hydrogenation and photocatalytic oxidation over the bifunctional Rh/WO3catalyst, *J. Environ. Chem. Eng.*, 2024, **12**(2), 11202.

53 P. C. Quero-Jiménez, A. Hernández-Ramírez, J. Luis Guzmán-Mar, M. Villanueva Rodríguez, D. A. Pino-Sandoval and L. Hinojosa-Reyes, Applicability of NH2-MOF235(Fe)-derived α-Fe2O3/ZnO photocatalyst synthesized by the microwave-assisted method in the degradation of a mixture of phenolic compounds, *J. Photochem. Photobiol., A*, 2024, **446**(1), 115154.

54 X. Dang, R. Yang, Z. Wang, S. Wu and H. Zhao, Efficient visible-light activation of molecular oxigen to produce hydrohen peroxide using P-doped g-C_3N_4 hollow spheres, *J. Mater. Chem. A*, 2020, **8**, 22720–22727.

55 H. Zhang, L. Liu, H. Zhang, Y. Wan and J. Luo, Biomimetic-photo-coupled catalysis for boosting H_2O_2 production, *Chem. Eng. J.*, 2024, **483**, 149183.

56 G. Yu, K. Gong, C. Xing, L. Hu, H. Huang, L. Gao, D. Wang and X. Li, Dual P-doped site modified porous g-C_3N_4 achieves high dissociation and mobility efficiency for photocatalytic H_2O_2 production, *Chem. Eng. J.*, 2023, **461**, 142140.

57 M. Fernandes, D. Hoefling Souza, R. Oliveira Henriques, M. Vicente Alves, E. Skoronski and A. Furigo Jr., Obtaining soybean peroxidase from soybean hulls and its application for detoxification of 2,4-dichlorophenol contaminated water, *J. Environ. Chem. Eng.*, 2020, **8**, 103.